Contribution from the Department of Chemistry,
Cornell University, Ithaca, New York 14853

Binuclear and Polymeric Gold(I) Complexes

YUANSHENG JIANG, SANTIAGO ALVAREZ, and ROALD HOFFMANN*

Received September 7, 1984

Qualitative molecular orbital studies on a model binuclear Au(I) compound with two bidentate ligands and a metal–metal bond, $[Au_2(S_2PH_2)_2]_2$ show that the Au···Au bonding interaction may be accounted for through s + p_z + d_{z^2} mixing, as for other d^{10} metal complexes; the same orbitals are able to form additional bonds along the Au–Au axis, leading to extension of the molecule into a chain or to Au(II) compounds via oxidative-addition reactions. The metal–ligand bonds, however, have no significant contribution from the metal d orbitals. Two different distortions that destroy the planarity of the chelate rings are analyzed: A D_2 ring puckering providing an increase in the SPS angles adds stability to the molecule, the driving force for this distortion being the minimization of the sulfur–sulfur lone pair repulsions. If the S donor atoms are replaced by isoelectronic CH_2 groups, a flapping of the PH_2 groups (C_{2h} distortion) is preferred. The study of the electronic structure of a dimer $[Au_2(S_2PH_2)_2]_2$ allows an easy understanding of the band structure diagrams calculated for the polymer $[Au_2(S_2PH_2)_2]_n$. Both in the dimer and in the polymer the staggered conformation is seen to be more stable than the eclipsed one. Some ways to stabilize an eclipsed chain are suggested on the basis of its band structure.

The inorganic and organometallic chemistry of gold cannot yet match in its richness the almost mythical role of the element in the history of human culture. Nevertheless, over the last decade many new compounds involving gold atoms in various oxidation states, bound by diverse ligands, have been synthesized. The chemistry of these compounds is summarized in monographs and review papers.[1-4] Also, some research on the bonding of certain gold compounds has been reported.[5-8]

Several bicyclic Au(I) compounds of structure **1** have been

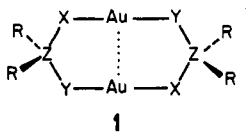

1

synthesized with Z = P and X = Y = S;[9,10] X = S, Y = CH_2;[11] X = Y = CH_2;[12,13] or R_2Z = R_2N, X = Y = S.[9] A similar compound with X = PR_2 and Y = S, but forming six-membered rings, is also known,[14] as well as related Cu(I) and Ag(I) compounds.[15] Several structural features appear in these molecules: the chelate rings are often puckered and some of them form chains.[9-11]

Table I. Structural Data for Binuclear Gold(I) Compounds

compd	chelate ring size	Au–Au dist, Å	XAuY angle, deg	angle between XAuY gps, deg	ref
$[Au_2(S_2P(OC_3H_7)_2)_2]_n$	5	3.04	174	38.0	10
$[AuS(CH_2)_2PEt_2]_2$	6	3.104	173.5	29.5	14
$[AuS_2NC(C_3H_7)_2]_2$	5	2.76	180.0	50.0	9
$[Au(CH_2)_2P(Et)_2]_2$	5	3.023	179.0	0	12
$[Au(CH_2)_2PSPH_2]_2$	5	3.04			11
$[Au(CH_2)_2PMe_2]_2$	5	3.005	177		13a
$Ba[Au_2SnS_4]$	5	2.98	170.9, 178.6		13c
$[Ph_4P][Au(WS_4)]_2$	5		167.2		13d

In this paper we study those bicyclic gold(I) compounds with structure **1** and their ability to form polymers. This work is part of a continuing effort of our group to provide conceptual models for bridging monomer, oligomer, and polymer extended structures. The Au(I) complexes are a good example of the continuity of molecular and extended bonding.

Some structural information on the binuclear complexes of type **1** is collected in Table I. Several structural features merit our attention: (a) Each gold atom is surrounded by two donor atoms in a linear way. (b) Both gold atoms are weakly bonded with a typical bond distance of 3.0 Å, except for the dithiocarbamate, which shows a quite shorter bond (2.76 Å). (c) The chelate rings are not planar, two types of ring puckering being observed: one in which all the metal and donor atoms lie in a plane but the bridging Z atom is significantly displaced out of the plane, observed only for the carbene derivative, and another one in which the two MXY fragments are rotated with respect to each other. (d) Some compounds form chains,[9-11] the successive units usually being in a rotated conformation as in other known Au(I) dimers or chains in which the repeat unit is a linear ML_2 group.[16]

We will start looking at a simple model of a binuclear compound (structure **1**, with R = H), assuming a planar bicyclic system, and study later the ring distortions. The ability of the binuclear compound to dimerize will provide us with a stepwise description of the bonding in the linear chains.

Bonding in the Planar Bicyclic Au_2 System

The model system we choose to examine first is $Au_2(S_2PH_2)_2$, with a geometry idealized from the observed structures. The

(1) Schmidbaur, H. "Gmelin's Handbuch der Anorganischen Chemie"; Springer-Verlag: Berlin and New York, 1980; Au-Org. Comp.
(2) Puddephatt, R. J. "The Chemistry of Gold"; Elsevier: Amsterdam, 1978.
(3) Schmidbaur, H. *Angew. Chem., Int. Ed. Engl.* **1976**, *15*, 728–740.
(4) Schmidbaur, H.; Dash, K. C. *Adv. Inorg. Chem. Radiochem.* **1982**, *25*, 239–266.
(5) Komiya, S.; Albright, T. A.; Hoffmann, R.; Kochi, J. *J. Am. Chem. Soc.* **1976**, *98*, 7255–7265.
(6) Komiya, S.; Albright, T. A.; Hoffmann, R.; Kochi, J. *J. Am. Chem. Soc.* **1977**, *99*, 8440–8447.
(7) Mingos, D. M. P.; *Proc. R. Soc. London, Ser. A* **1982**, *A308*, 75–83.
(8) Evans, D. G.; Mingos, D. M. P. *J. Organomet. Chem.* **1982**, *232*, 171–191.
(9) Hesse, R.; Jennische, P. *Acta Chem. Scand.* **1972**, *26*, 3855–3864.
(10) Lawton, S. L.; Rohrbaugh, W. J.; Kokotailo, G. T. *Inorg. Chem.* **1972**, *11*, 2227–2233.
(11) Mazany, A. M.; Fackler, J. P. *J. Am. Chem. Soc.* **1984**, *106*, 801–802.
(12) Schmidbaur, H.; Mandl, T. E.; Richter, W.; Bejenke, V.; Frank, A.; Huttner, G. *Chem. Ber.* **1977**, *110*, 2236–2241.
(13) (a) Fackler, J. P.; Basil, J. D. In "Inorganic Chemistry: Towards the 21st Century"; Chisholm, M. H., Ed.; American Chemical Society: Washington, D.C., 1983; ACS Symp. Ser. No. 211, p 201. (b) Schmidbaur, H.; Scherm, H. P.; Schubert, U. *Chem. Ber.* **1978**, *111*, 764–769. (c) Teske, C. L. *Z. Anorg. Allg. Chem.* **1978**, *445*, 193. (d) Müller, A.; Dornfeld, H.; Henkel, G.; Krebs, B.; Viegers, M. P. A. *Angew. Chem., Int. Ed. Engl.* **1978**, *17*, 52.
(14) Crane, W. S.; Beall, H. *Inorg. Chim. Acta* **1978**, *31*, L469–470.
(15) (a) Schmidbaur, H.; Adlkofer, J.; Buchner, W. *Angew. Chem., Int. Ed. Engl.* **1973**, *12*, 415–416. (b) Nardin, G.; Randaccio, L.; Zangrando, E. *J. Organomet. Chem.* **1974**, *74*, C23–C25. (c) Brown, I. D.; Dunitz, J. D. *Acta Crystallogr.* **1961**, *14*, 480–485. (d) Papasergio, R. I.; Raston, C. L.; White, A. H. *J. Chem. Soc., Chem. Commun.* **1984**, 612–613; *Ibid.* **1983**, 1419.
(16) (a) Arai, G. J. *Recl. Trav. Chim. Pays-Bas* **1962**, *81*, 307–312. (b) Corfield, P. W. R.; Shearer, H. M. M. *Acta Crystallogr.* **1967**, *23*, 156–162. (c) Hollis, S. L.; Lippard, S. J. *J. Am. Chem. Soc.* **1983**, *105*, 4293–4299. (d) Drew, M. G. B.; Riedl, M. J. *J. Chem. Soc., Dalton Trans.* **1973**, 52–55. (e) Strähle, J.; Hiller, W.; Conzelmann, W. *Z. Naturforsch, B: Anorg. Chem., Org. Chem.* **1984**, *39B*, 538–541. (f) Cooper, M. K.; Mitchell, L. E.; Henrick, K.; McPartlin, M.; Scott, A. *Inorg. Chim. Acta* **1984**, *84*, L9–L10.

0020-1669/85/1324-0749$01.50/0

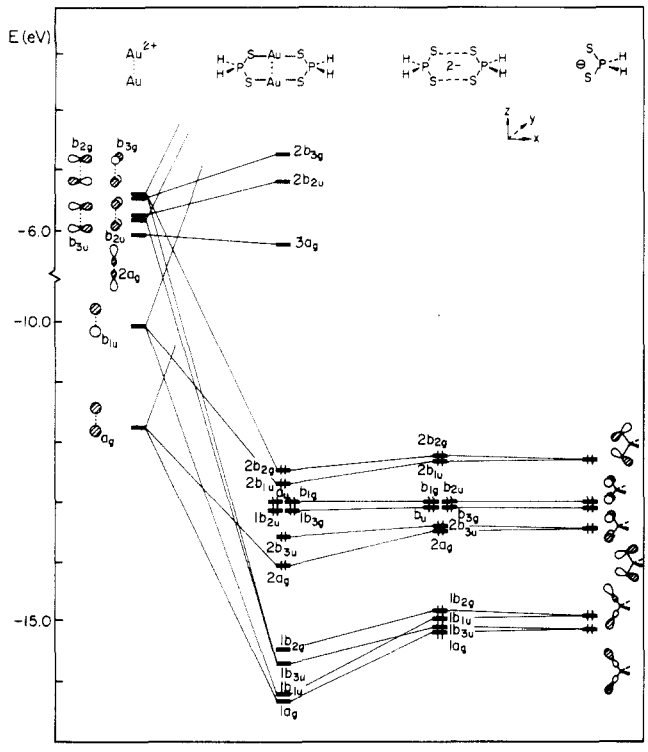

Figure 1. Orbital interaction diagram for Au_2^{2+} with two $S_2PH_2^-$ ligands, forming a planar bicyclic system. No d orbitals are included.

details of the geometry and the extended Hückel calculations used throughout this paper are given in the Appendix. The dimer may be thought of as being formed from a Au_2^{2+} stick and two bidentate $S_2PH_2^-$ ligands, as in **2**.

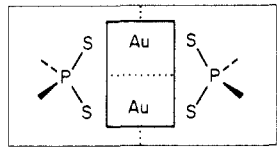

2

The Au_2^{2+} grouping may be built from the atoms. At first sight one might think that no metal–metal bonding and only repulsion may occur between two d^{10} ions such as Cu, Ag, or Au(I). But, in fact, substantial s and p mixing into the d block gives some such bonding. This has been analyzed previously[17] and is responsible for the general tendency of Cu, Ag, and Au(I) ions to cluster. In the particular case of Au_2^{2+} at a separation of 3.04 Å, the Au–Au overlap population is small and positive, 0.0435.

While d, s, and p hybridization on gold is important for Au–Au bonding, the discussion of the bonding of this Au_2^{2+} unit with other ligands is facilitated by choosing a simpler model. In it, the Au atoms bear only s and p orbitals. We will later restore the Au d orbitals. Thus, the orbitals of the Au_2^{2+} fragments presented in Figure 1, labeled in the D_{2h} point group, are all empty. $1a_g$ and b_{1u} are the bonding and antibonding combinations of 6s, and higher in energy are $2a_g$ (σ_z) and the π-bonding (b_{2u}, b_{3u}) and π-antibonding (b_{2g}, b_{3g}) orbitals formed from gold 6p.

Each $S_2PH_2^-$ ligand has three lone pairs on each sulfur atom, shown in localized form in **3**. With two sulfurs per ligand, one comes to six high-lying orbitals per ligand, illustrated at the right of Figure 1. Very weak interaction between the $S_2PH_2^-$ ligands then generates the 12 potential donor orbitals of the two ligands. We are set to remove the inner box separating Au_2^{2+} and $(S_2PH_2)_2^{2-}$ fragments in **2**.

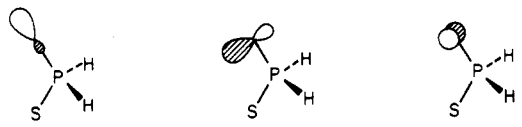

3

Two sets of donor orbitals of σ type (**3a,b**) span the identical representations $A_g + B_{2g} + B_{1u} + B_{3u}$. These orbitals find a symmetry match in the Au_2 side of the diagram, and for each of these symmetry species, a typical three-orbital interaction pattern appears, producing a bonding, a nonbonding, and an antibonding MO. We will focus on the bonding and nonbonding levels of a_g symmetry. The σ lone pairs of the sulfur atoms rehybridize giving place to the reoriented lone pair **4a** and the S–Au bond **4b**; the

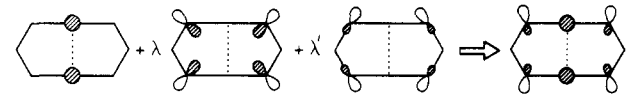

4a

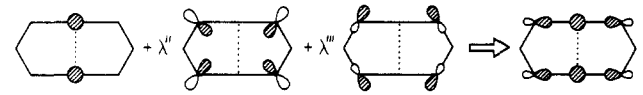

4b

same type of rehybridization is operative for the remaining σ orbitals (b_{2g}, b_{1u}, b_{3u}) and therefore the $1a_g$, $1b_{1u}$, $1b_{3u}$, and $1b_{2g}$ orbitals are just the sulfur σ-donor orbitals, while $2a_g$, $2b_{1u}$, $2b_{3u}$, and $2b_{2g}$ are sulfur lone pair orbitals.

Of the four sulfur π lone pair orbitals of the ligands, only two are allowed by symmetry to interact with the Au_2 orbitals. This π interaction is very weak but can be detected by the increased energy of the $2b_{2u}$ and $2b_{3g}$ MO's relative to the corresponding gold stick orbitals.

The levels in Figure 1 can now be characterized. The lowest four are Au–S σ-bonding orbitals. Above these are eight orbitals that are predominantly S lone pairs, four σ and four π. Then a gap is reached, between the filled and unfilled levels of a neutral $Au(S_2PH_2)_2$. Above the gap we find the $3a_{1g}$, Au–Au bonding but really hybridized away from the other Au. And above it $2b_{2u}$ and $2b_{3g}$, Au–Au π and π^*.

What happens if we now reintroduce the d orbitals of the gold atoms? Not much as far as the metal–ligand interactions are concerned: the d block appears in the region between $1b_{2g}$ and $2a_g$, around −15 eV, and most of the MO's discussed above incorporate some d character, but the previous description of the metal–ligand bonding is still valid. Effectively, the gold–gold bond cannot be explained without d orbitals, and consequently all the results reported, except the diagram in Figure 1, were obtained with the inclusion of the d orbitals.

It might be noted here that ^{197}Au Mössbauer measurements support the primary involvement of Au 6s and 6p orbitals in bonding with the sulfurs in one of these binuclear complexes.[13d]

To anticipate the subsequent discussion we might think about stacking or polymerization of these dimers and the donor and acceptor characteristics of the binuclear unit that might enhance such stacking. First of all let us specify the polymerization process schematically as **5**, with no implication made of the rotational conformation of each unit relative to its neighbor. The connectivity is σ type, as it is in the platinocyanides, **6**. So we must look for donor and acceptor orbitals of σ symmetry in the monomer. The idea behind this is the usual one of maximizing two-electron-bonding interactions between monomer units, indicated schematically in **7**. In the platinocyanides the donor orbital is the z^2 and the acceptor a $z + \lambda(CN\ \pi^*)$ combination. What are likely to be the corresponding orbitals in the Au polymers of type **5**?

(17) (a) Mehrotra, P. K.; Hoffmann, R. *Inorg. Chem.* **1978**, *17*, 2187–2189. (b) Dedieu, A.; Hoffmann, R. *J. Am. Chem. Soc.* **1978**, *100*, 2074, 2079.

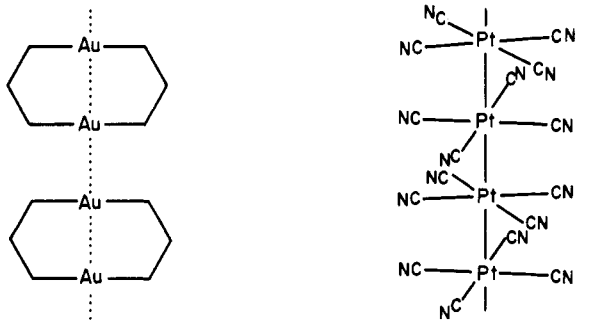

5 6

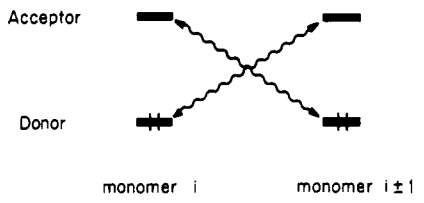

7

We see in Figure 1 a relatively low-lying $3a_g$, quite localized on gold. This is likely to have substantial acceptor power. The donor capability will be found in the two predominantly z^2 combinations not shown in the figure but schematically of type **8**. The

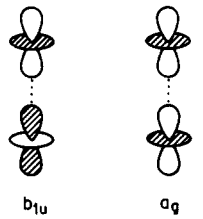

8

s,p mixing will make b_{1u} take on outward-reaching lone pair character. In addition to these, one of the orbitals we think of as S lone pair, the b_{1u}, will have a substantial admixture of Au_2 b_{1u}, the σ^* 6s combination. We will return to these orbitals later.

If the sulfur donor atoms are replaced by isoelectronic CH_2 groups, the resulting interaction diagram is essentially the same. The four σ interactions of the CH_2^- lone pairs with the s and p_x of the gold stick appear again although their relative order is not the same. Some minor differences are as follows: (a) The four π-type lone pairs in the sulfur donors (a_u, b_{1g}, b_{2u}, and b_{3g} in Figure 1) are now the C–H bonds and, consequently, appear at lower energy, below the d block. (b) The gold π_y orbitals (b_{2u} and b_{3g} empty orbitals) are less destabilized because of their weaker interaction with C–H bonds rather than S lone pairs. (c) The P–C σ orbitals appear at higher energy than the P–S ones due to electronegativity reasons, overlapping in the energy scale with the d block. (d) The lower set of σ-donor orbitals is now involved in C–H bonds and appear at lower energies. Thus, it is clear that our previous interaction diagram (Figure 1) can be used to study the bonding in both dithiophosphinato and dicarbenephosphinato complexes.

The Au(I) compounds easily undergo oxidative-addition reactions, producing shorter gold–gold bonds (~2.6 Å)[3,18,19] while adding a ligand to each gold atom, as in **9**. The orbital accounting

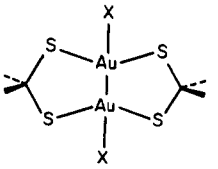

9

for this oxidative addition is simple and may be seen in Figure 2. The two ligands produce a_g and b_{1u} combinations, which interact well with a higher occupied $2b_{1u}$ and the LUMO $3a_g$ orbital of the unoxidized binuclear complex. The Au–Au bond order is increased by electron transfer out of $2b_{1u}$ and into $3a_g$ fragment orbitals. Interestingly, the HOMO–LUMO gap appears to be reduced on oxidative addition.

Ring Puckering

Two types of ring deformations are found in the binuclear gold complexes. They are sketched in **10**. The one that retains C_{2h}

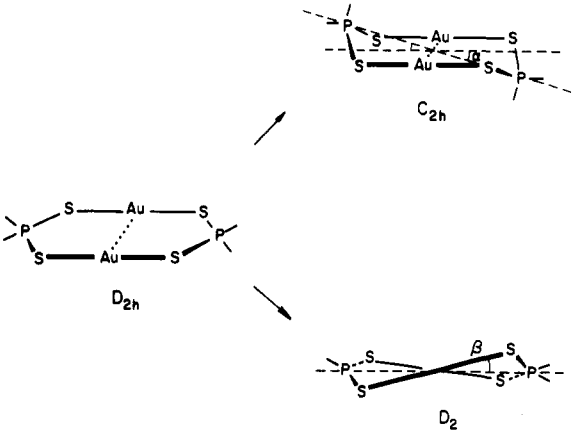

10

symmetry may be described simply as an out-of-plane displacement of both PH_2 groups. In our simulation of this conformation, all bond distances are kept constant and the parameter to be varied is the angle α, which measures the elevation (or depression) of the P atom; the AuSP angle depends on α and is the only other relevant parameter that is not fixed.

For the second kind of distortion, D_2 in **10**, the parameter to be varied is the relative rotation angle of the two AuS_2 groups around the Au_2 bond, β; again, all the bond distances are kept fixed through the puckering process, but the nonbonded S–S distance, as well as the SPS bond angle, increases with β.

The Walsh diagrams for both distortions are shown in Figure 3 where the symmetry labels corresponding to the undistorted molecule have been included in parentheses. For the C_{2h} distortion, the salient feature of the Walsh diagram is the decrease in energy of the b_g and a_u orbitals, indicating the onset of the σ interaction between the high-lying b_{2u} and b_{3g} empty orbitals of the gold stick and the ligands' formerly π lone pairs b_g and a_u (Figure 1). At the same time, however, the σ interactions of b_{2g} and b_{3u} orbitals decrease (these levels are too low to be seen in Figure 3), and as a result there is no significant variation in total energy for a reasonable degree of distortion.

Quite different are the results for the D_2 distortion. Here, the orbitals that experience an important decrease in energy are the sulfur σ pairs (see $2b_{2g}$ and $2b_{1u}$ in the Walsh diagram, Figure 3b). Let us recall that these lone pair MO's are metal–ligand nonbonding, but sulfur–sulfur antibonding **11**. Hence, as the two sulfur atoms on the same ligand are separated by the distortion, the antibonding character of the orbitals in **11** decreases and so

(18) (a) Schmidbaur, H.; Franke, R. *Inorg. Chim. Acta* **1975**, *13*, 85–89. (b) Schmidbaur, H.; Mandl, J. R.; Frank, A.; Huttner, G. *Chem. Ber.* **1976**, *109*, 466–472. (c) Schmidbaur, H.; *Acc. Chem. Res.* **1975**, *8*, 62–70. (d) Schmidbaur, H.; Wohleben, A.; Wagner, F. E.; Van de Vondel, D. F.; Van der Kelen, G. P. *Chem. Ber.*, **1977**, *110*, 2758–2764.

(19) (a) Beurskens, P. T.; Blaauw, H. J. A.; Cras, J. A.; Steggerda, J. J. *Inorg. Chem.* **1968**, *7*, 805–810. (b) Beurskens, P. T.; Cras, J. A.; Steggerda, J. J. *Inorg. Chem.* **1968**, *7*, 810–813. (c) Calabro, D. C.; Harrison, B. A.; Palmer, G. T.; Moguel, M. K.; Rebbert, R. L.; Burmeister, J. L. *Inorg. Chem.* **1981**, *20*, 4311–4316. (d) Fackler, J. P.; Murray, H. H.; Basil, J. D. *Organometallics* **1984**, *3*, 821–822. (e) Fackler, J. P.; Basil, J. D. *Organometallics* **1982**, *1*, 871–873.

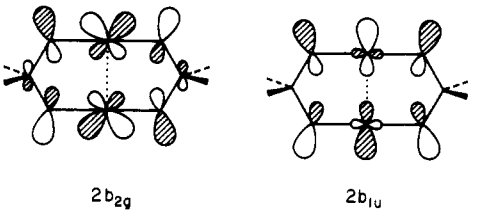

11

does their total energy, as seen in Figure 3. The same considerations apply for the lower sulfur σ lone pair MO's, $2b_{3u}$ and $2a_g$. As a result, the preferred distortion is D_2 with a minimum at $\beta = 17.5°$, quite close to the experimental value, $\beta = 19°$; the S–S distance for this angle is 3.33 Å while the experimental distance is 3.42 Å. As suggested by the topology of the orbitals in **11**, their small contributions from the metal d orbitals, and essentially sulfur–sulfur antibonding character, (a) the Au–Au overlap population varies very little with the distortion (Figure 5) and the corresponding bond length is expected to be almost insensitive to the degree of puckering (see Table I) and (b) the driving force for this distortion is the repulsive sulfur–sulfur interaction, as previously proposed,[10] which decreases from the planar situation (overlap population −0.090) to the optimal geometry (overlap population −0.047).

When the donor sulfur atoms are substituted by CH_2 groups, the behavior toward distortion is somewhat different: the protons bonded to the carbon atoms take electron density off what in sulfur were lone pairs. In consequence, the carbon–carbon repulsion in the planar conformation is much smaller than in the case of sulfur. The total energy curve for the D_2 motion (Figure 4 bottom) shows that only a very small stabilization is gained in this case. On the other hand, the C_{2h} puckering leads to a minimum at $\alpha = 15°$ corresponding to a chair conformation with AuCP angle of 110°, in the range of the experimentally observed values of 108–114°.[12] This stabilization can be explained as the preference for a staggered rather than an eclipsed conformation in the ethane-like $AuCH_2$–PH_2R, as shown in a Newman projection along the C–P bond in **12**, the calculated dihedral angle τ being 56°.

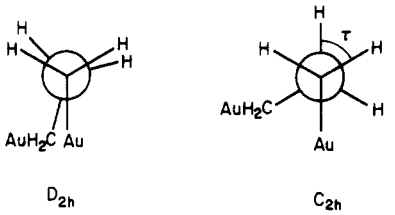

12

Electronic Structure of the Dimer $[Au_2(S_2PH_2)_2]_2$

Before discussion of the electronic structure of the polymer based on band calculations, it is worthwhile to take a look at the dimer in order to understand how two units of **1** can bond together. The study of the dimer will also allow us to show how the electronic structure of a dimer provides sufficient information to make qualitative predictions of the band structure of the related polymer; in particular, we will be able to say which orbitals are going to produce wide bands, what is the composition of each band at the center and edges of the Brillouin zone, and whether a particular band will present a positive or a negative slope.

As we have seen in the preceding section, the ring puckering may change the order of the molecular orbitals but the essential features of the interaction diagram for the planar molecules (Figure 1) are retained. Hence, for the sake of simplicity, all the calculations on the dimer and polymer have been carried out by using the planar geometry. Two conformations will be considered for the dimer: eclipsed **13** and staggered **14**.

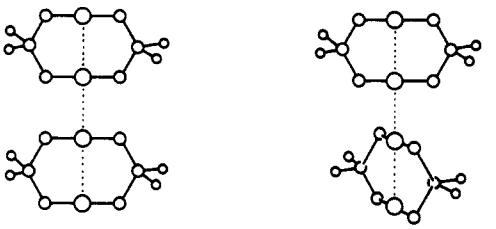

13 **14**

The molecular orbitals of the dimer would be expected to be, to a first approximation, the in-phase and out-of-phase combinations of the equivalent orbitals of both monomers. The symmetry labels of such combinations in the eclipsed dimer are shown in Table II where the superscripts i and o mean in-phase and out-of-phase combinations, respectively, and will be of some use later on.

It was hinted at in the Introduction that one should look for donor–acceptor interactions. The group-theoretical considerations of Table II show that the LUMO's $3a_g$ (see Figure 1) of both monomers produces combinations of the same symmetry as those of one of the highest occupied orbitals, $2b_{1u}$, **8**; the same applies for the antibonding combination of the z^2 orbitals in the monomers. With focus on the metal axis, the interactions of these orbitals are sketched in **15**, where no bond is formed; however, mixing of

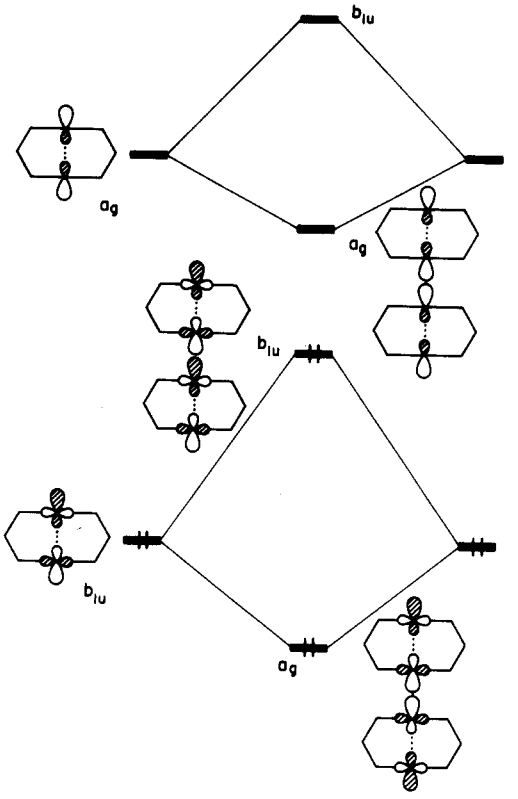

15

both a_g orbitals of the dimer, **16**, increases the intermolecular bonding character of the occupied orbital while decreasing the intermolecular bonding character of the empty one, and the result is some intermolecular gold–gold overlap population (0.019, compared to 0.025 for the intramolecular bond). This is the same kind of interaction that is operative in the intramolecular Au–Au bond and the one that applies for the bonding in most formally d^{10} metal complexes.[17]

Table II also allows us to deduce the splitting of the monomer MO's on formation of an eclipsed dimer. For example, the second column of the table tells that the b_{2g} orbitals of both monomers form a b_{3u} bonding and a b_{2g} antibonding combination (**17**).

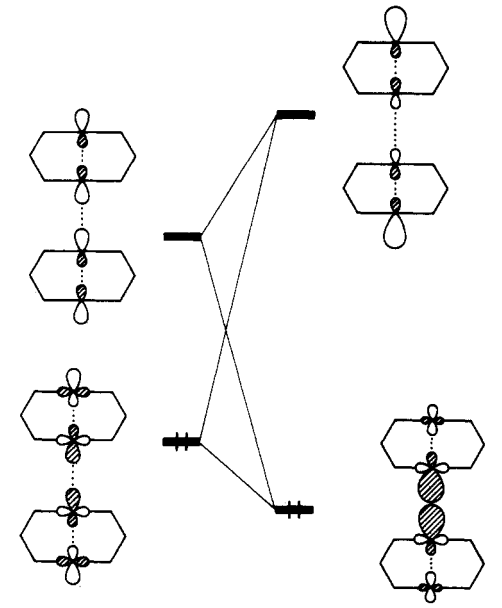

16

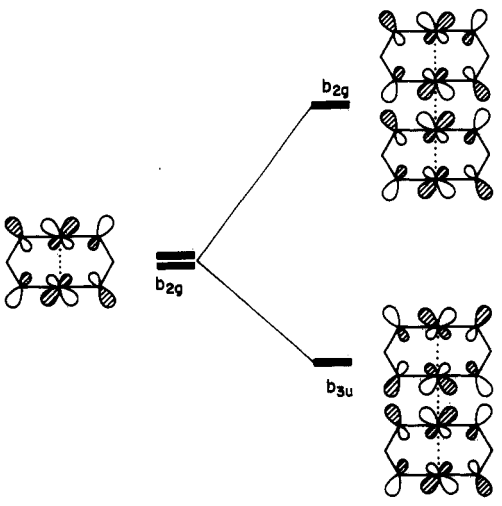

17

By examining Table II and the nodal character of the orbitals, one can roughly estimate the relative magnitude of the splitting corresponding to each column in Table II. The higher occupied MO's of the monomer (b_{2g}, b_{1u}, a_u, b_{1g}, b_{2u}) have comparable population and nodal character at the sulfur atoms, and thus differences in the splitting will be mainly determined by the gold–gold interactions. For d orbitals we can expect the order $\sigma > \pi > \delta$. On the other hand, the b_{2u} and b_{3g} splittings will be very small since the mixing of gold p character is very small. The resulting qualitiative sequence for the splitting of these levels in the dimer is thus b_{1u}, a_g (σ) > b_{2g}, b_{3u} (π) > a_u, b_{1g} (δ) > b_{3g}, b_{2u} (σ), which is indeed found in the calculated result for the dimer (Figure 6).

So far so good, but the overall overlap population between two monomers is −0.201, indicative of a net repulsive interaction; a look at the form of the $2b_{1u}$ orbital, **11**, a sulfur lone pair orbital facing directly the second monomer, makes the filled orbital interaction represented in **15** highly repulsive. It is therefore obvious that a rotation leading to the staggered conformation should relieve this repulsive interaction. The overlap population becomes +0.018.

Let us follow through with the group-theoretical analysis for the staggered dimer. The symmetry is D_{2d}, and the perpendicular conformation almost eliminates the mutual interaction between

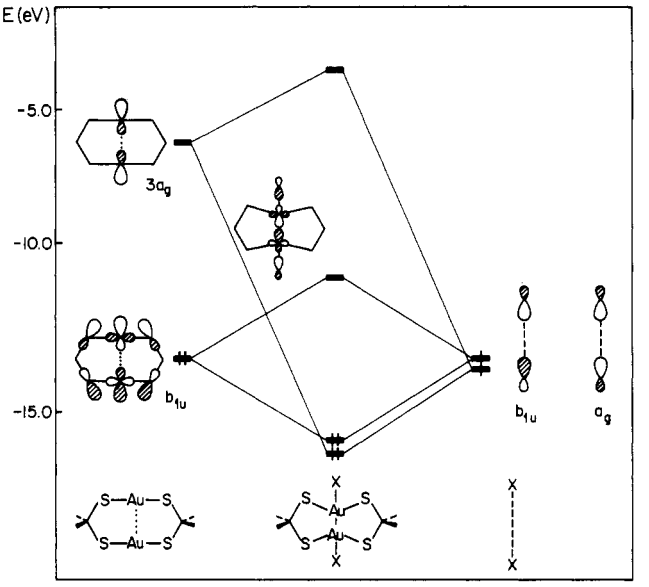

Figure 2. Partial interaction diagram for oxidative addition of X_2 to $[Au_2(S_2PH_2)_2]$.

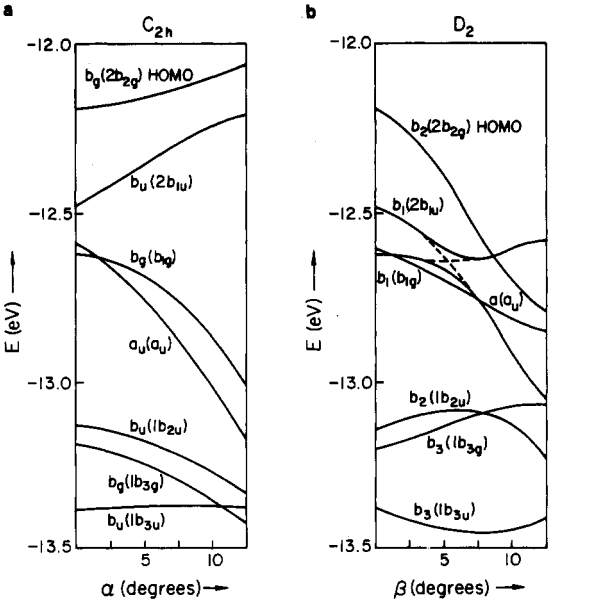

Figure 3. Walsh diagrams for the ring-puckering distortions **10** of $[Au_2(S_2PH_2)_2]$: (a) C_{2h} mode; (b) D_2 mode.

Table II. Eclipsed Dimer MO's as Combinations of Monomer MO's

monomer MO	b_{2g}	b_{1u}	a_u	b_{1g}	b_{2g}	b_{3g}	b_{3u}	a_g
bonding combin	b_{3u}^o	a_g^o	b_{1g}^o	b_{1g}^i	b_{2u}^i	b_{2u}^o	b_{3u}^i	a_g^i
antibonding combin	b_{2g}^i	b_{1u}^i	a_u^i	a_u^o	b_{3g}^o	b_{3g}^i	b_{2g}^o	b_{1u}^o

Table III. Staggered Dimer MO's as Combinations of the Orbitals of Two Perpendicular Monomers and Their Relative Splittings

		dimer MO		
monomer MO	Au–Au bond type	bonding	antibonding	splitting
b_{2g}, b_{3u}, b_{3g}, b_{2u}	π	e		0
b_{1u}, a_g	σ	a_1	b_2	lg
a_u, b_{1g}	δ	b_1	a_2	sm

ligands. Thus, gold–gold interactions between monomers are the only factor determining the splitting of levels. We can again obtain

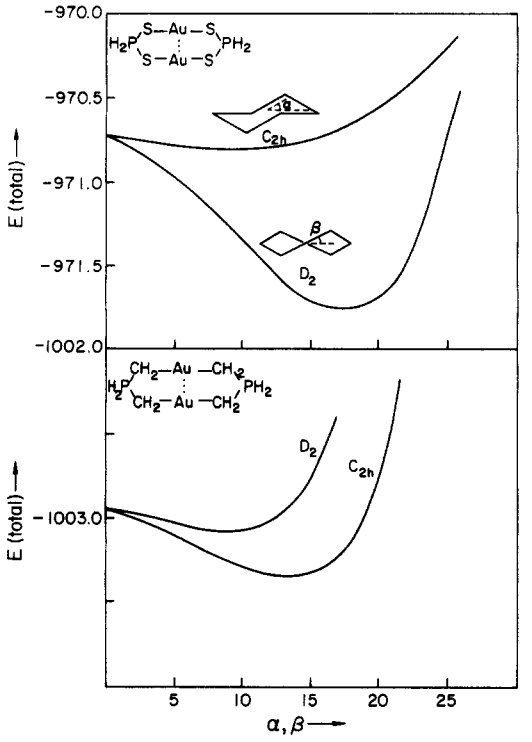

Figure 4. Potential energy curves for the ring-puckering distortions **10** of $[Au_2(S_2PH_2)_2]$ (top) and $[Au_2((CH_2)_2PH_2)_2]$ (bottom).

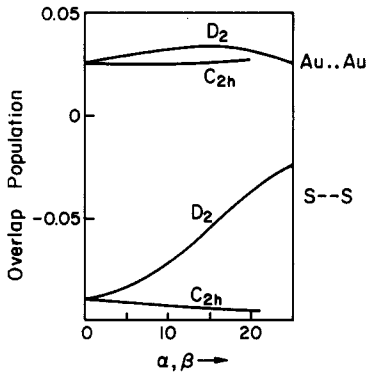

Figure 5. Variation of the Au–Au and S--S overlap populations in $[Au_2(S_2PH_2)_2]$ with the ring distortions of C_{2h} and D_2 symmetry.

the MO's of the dimer in terms of the orbitals of two mutually perpendicular monomers and qualitatively predict their relative splittings, using the $\sigma > \pi > \delta$ criterion for Au–Au interactions (Table III). The level ordering predictions are confirmed by the calculated sequence of levels of Figure 6. These levels will be the source of the band structures of eclipsed and staggered infinite polymers that we will calculate in the next section.

The staggered conformation for the dimer is calculated to be more stable than the eclipsed one. Two reasons can be found for this difference, although it is not possible to elucidate with our calculations their relative importance, as previously pointed out for another d^{10} system:[17b] the sulfur-sulfur lone pair repulsion between monomers and an incipient Au–Au π bond.

The argument based on S–S repulsion being obvious, let us focus on the π interaction. As the gold p_x orbitals are highly destabilized because of the σ interaction with the donor atoms, the only empty gold π orbitals available are p_y ($2b_{2u}$ and $2b_{3g}$ in Figure 1). On the other hand, the filled orbitals available for π bonding are $1b_{2g}$ and $1b_{3u}$, both perpendicular to the plane of the molecule. Hence, no π interaction is allowed for the eclipsed dimer. If one of the monomers is rotated, the π interactions become allowed and some stabilization is gained, as a significant increase in the intermolecular Au–Au overlap population indicates (from 0.019 in the eclipsed from to 0.029 in the staggered one). As both $2b_{2u}$ (π in the monomer) and $2b_{3g}$ (π^* in the monomer) are equally populated, no great variation in the intramolecular Au–Au bond distance appears (compare Au–Au bond distance of 3.01 Å in the staggered chain[10] with 3.04 Å in a chain with a smaller rotation angle[11]). However, the intermolecular interaction populates only its bonding π combinations, in agreement with the shorter intermolecular Au–Au distance (3.04 Å) in the staggered chain[10] as compared to that in a chain with a smaller rotation angle (3.22 Å).[11]

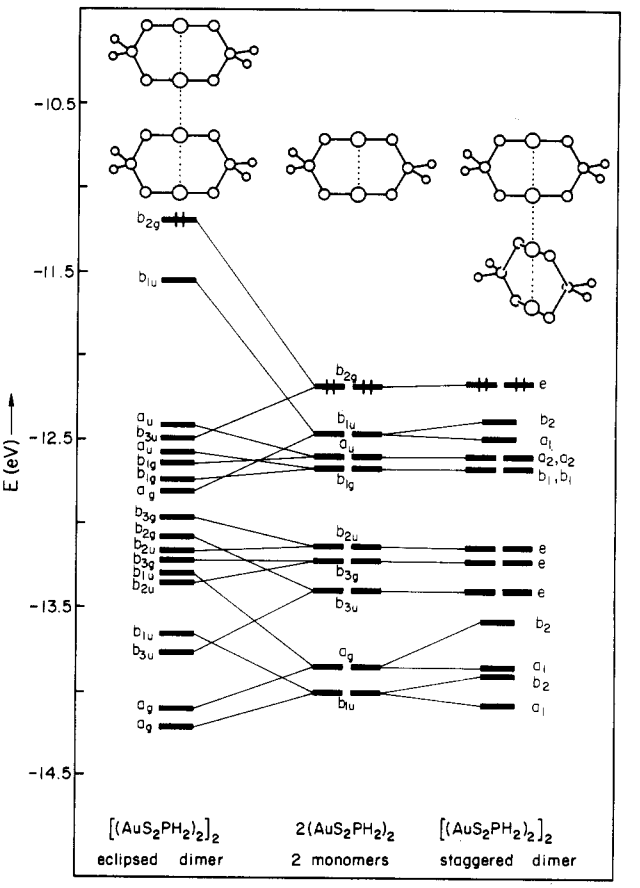

Figure 6. Orbital splitting pattern for two monomers of $[Au_2(S_2PH_2)_2]$ interacting in an eclipsed and a staggered way.

We are now ready to examine some infinite extended structures.

Band Structure and Stability of $[Au_2(S_2PH_2)_2]_n$

Various chain conformations are possible for the polymer; the three shown in **18** will be considered here for the model polymer,

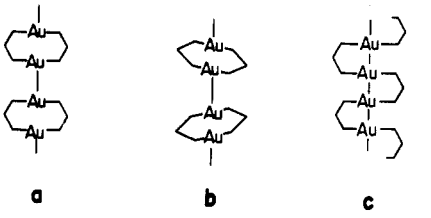

18

where the bulky OC_3H_7 of the real polymer[10] have been replaced by hydrogen atoms and a planar ring conformation is again assumed. From our results on the dimer we can anticipate that the all eclipsed conformation **18a** should be less stable than the staggered one due to sulfur–sulfur lone pair repulsions, but we want to look at the eclipsed case first because it is simpler to analyze.

Let us first obtain a rough estimate of the band structure on the basis of information we already have for an eclipsed dimer

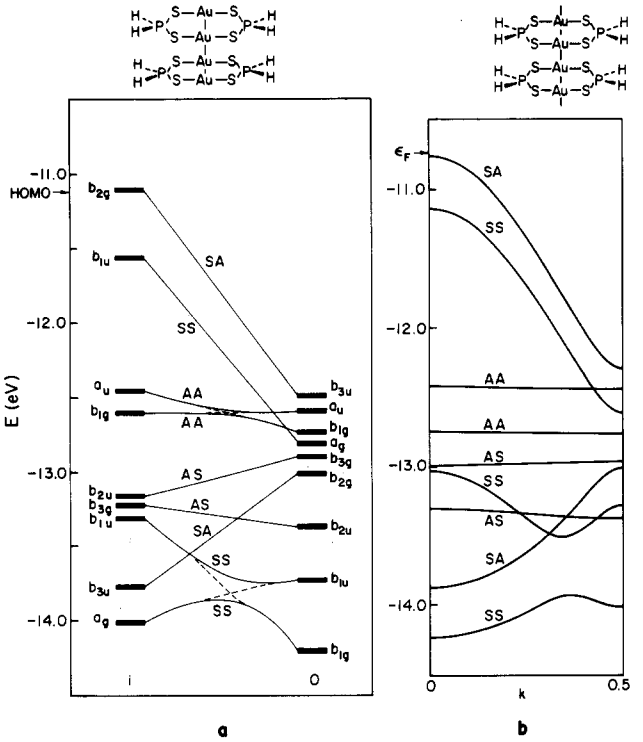

Figure 7. Bandlike arrangement of the molecular orbitals of an eclipsed dimer $[Au_2(S_2PH_2)_2]_2$ (a) and tight-binding band calculation for the polymer $[Au_2(S_2PH_2)_2]_n$ with an eclipsed conformation (b). Only the higher occupied MO's and bands are shown.

and compare this later with a tight-binding calculation. We then represent the center of the Brillouin zone ($k = 0$) with the in-phase combinations of the monomers' MO's (i superscript in Table II) at the left side of Figure 7a and the edge of the Brillouin zone ($k = \pi/a$) with the out-of-phase combinations of the same orbitals (o superscript in Table II) at the right side of Figure 7a. By linkage of each level at the left with the level at the right arising from the same monomer MO, the qualitative band diagram is generated. Finally, we classify the levels with respect to their symmetry in the C_{2v} point group.[20] Two avoided crossings then appear (for AA and SS levels), and the qualitative band diagram is complete. In Figure 7b is presented the computed band structure of the polymer, essentially the same as Figure 7a. Note how simply the band structure is generated.

This chain compound is calculated to be an insulator, since the lowest empty band (not shown in Figure 7) is around 4.5 eV above the Fermi level. The large dispersion shown by the two highest occupied bands (between −11.5 and −12.5 eV in Figure 7b) gives the band description of the previously found reason for the instability of the eclipsed dimer: as the antibonding combinations of the highest occupied orbitals of the monomer, $k = 0$, are destabilized more than their bonding combinations ($k = 0.5$) are stabilized, the net interaction is repulsive (the typical two orbitals–four electrons interactions in molecules). However, there is still some hope that such an eclipsed chain could be synthesized. Partial oxidation would remove electrons from the upper part of the valence band that is composed of antibonding combinations of the $2b_{2g}$ MO. As a result, the repulsive interaction should become an attractive one, the resulting partially filled band giving rise to metallic electrical conductivity.

An interesting possibility is more extensive oxidation to the Au(II) or even the Au(III) state. From the band structure of Figure 7 we might expect half-filled SS and SA bands, and a possible Peierls distortion in the former case, but still more intriguing is the choice between two isomeric structures of type **19**.

(20) This is the point group to which any combination of monomer orbitals in the chain (i.e., any point in k space) belongs. The labels S and A refer to symmetric and antisymmetric orbitals with respect to both symmetry planes in the chain: the first letter corresponds to the plane of the molecule (xz in **10**) and the second one to the perpendicular plane (yz in **10**).

Table IV. Energies and Overlap Populations for Three Isomers of $[Au_2(S_2PH_2)_2]_n$

		D_{2h} (eclipsed)	D_{2d} (staggered)	C_{2h} (zigzag)	monomer
av E/unit cell, eV		2.29	0.14	2.30	0
band gap, eV		4.25	5.77	4.25	6.29
Au–Au overlap populn	intramolecular	0.025	0.024	0.025	0.025
	intermolecular	0.019	0.030	0.025	
S--S overlap populn	intramolecular	−0.090	−0.090	−0.076	−0.090
	intermolecular	−0.082	−0.001	−0.076	

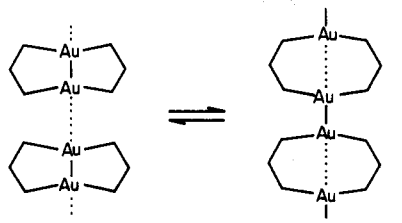

19

A closer look at the composition of these two bands sketched in **20** is illustrative. Two features differentiate these orbitals from

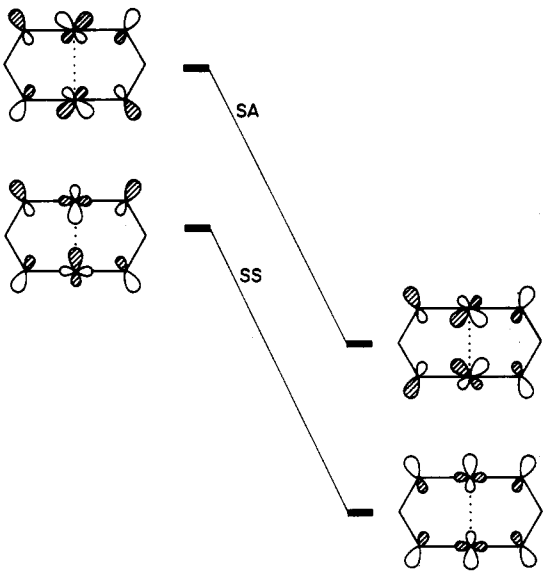

20

their equivalents in a dimer: the lower parts of the bands arise from different monomer's orbitals than the higher part, due to avoided crossings with lower bands of the same symmetries, and in two cases the metal orbitals are rehybridized inward within the cyclic dimer. The same principle used for a dimer in **16** applies here: mixing with higher (unoccupied) bands tends to minimize the intercell antibonding character of the highest SS and SA bands in Figure 7.

For the Au(II) oxidation state the trend is clear: the electrons removed upon oxidation were occupying orbitals strongly Au–Au antibonding within the unit cell, strongly sulfur–sulfur antibonding, and slightly Au–Au antibonding between nearest neighbors. The intermolecular Au–Au bond should thus be strengthened and the intermolecular sulfur–sulfur repulsion turned into a weakly at-

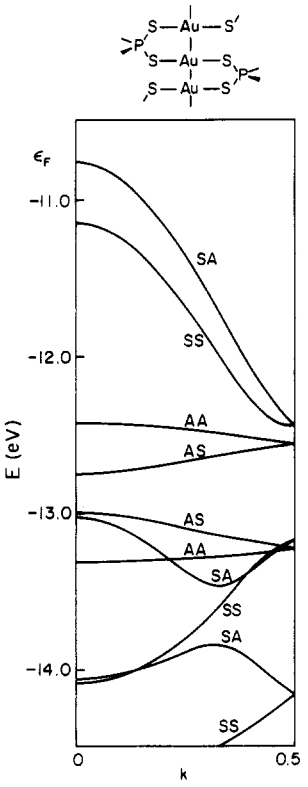

Figure 8. Band structure of the zigzag form of the polymer $[Au_2(S_2PH_2)_2]_n$.

tractive interaction, stabilizing the chain **19a**.

If both SA and SS were empty for a Au(III) chain, then the intermolecular Au–Au bonding should be enhanced, producing a fully singly bonded chain. The crossing of the SS band with a nonbonding AA one prevents this from happening in our calculations, and simultaneously changing the intra- and the intermolecular Au–Au distances while keeping the ligands frozen, we find the following equilibrium distances for the intra- and intermolecular bands respectively: Au(I), 3.0 and 3.1; Au(II), 2.9 and 3.2; Au(III), 2.8 and 3.3. The intermolecular sulfur–sulfur overlap population is in the latter case clearly positive, suggesting the possibility of forming a new sulfur–sulfur bond in a process formally related to the tetrathionaphthalene oxidative addition[21] to a metal complex **21**. Perhaps one should encourage aggregation of this type by attempting to remove the axial halides of known Au(II) compounds.

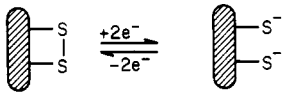

21

The situation is similar for the C_{2h} zigzag chain **15**, since the sulfur–sulfur repulsions remain the same; hence, its energy is very close to that of the previously discussed eclipsed chain (see Table IV for a comparison of the various polymers). The band structure for the zigzag chain is shown in Figure 8. Now the plane perpendicular to the molecule is not a symmetry element, but a new symmetry operation appears: a 2_1 screw axis. The second symmetry label for the bands refers to this screw axis. The different symmetry introduces some minor changes in the band diagram, but the general aspect of both diagrams (Figures 7b and 8) is the same and the conclusions drawn for the eclipsed chain hold for the zigzag polymer as well.

In the staggered chain the interactions between the highest occupied MO's are quenched, as discussed for the dimer. The higher occupied bands show very little dispersion if any (Figure 9). The electrical insulating character of the polymer is not expected to be altered through partial oxidation. The small dispersion in these bands was to be expected from the small splitting found for the staggered dimer (Figure 6). As anticipated, the energy per unit cell is smaller for the staggered chain than for the other two conformations considered (Table IV), but it is slightly larger than that of the monomer. This does not mean that the polymer should be expected to be unstable, but rather it is an artifact of the computational method used, which overestimates the two-orbital–four-electron interactions. Better indicators of the stability are the Au–Au and S--S intermolecular overlap populations, both favoring the staggered conformation (Table IV).

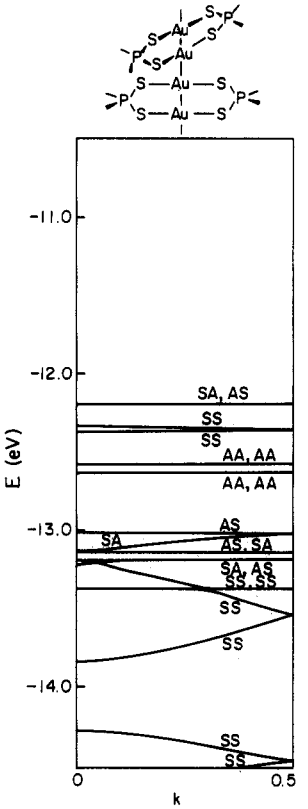

Figure 9. Band diagram for the staggered form of the polymer $[Au_2(S_2PH_2)_2]_n$.

Table V. Bond Distances (Å) and Angles (deg) for $[(AuS_2PH_2)_2]_n$ and $[Au(CH_2)_2PH_2]_2$

$[(AuS_2PH_2)_2]_n$				$[Au(CH_2)_2PH_2]_2$			
	dist		angle		dist		angle
Au–Au	3.04	HPH	100	Au–Au	3.02	HPH	100
Au–S	2.28			Au–C	2.10	HCH	99
S–P	2.00			C–P	1.79		
P–H	1.40			P–H	1.40		
S···S	3.42			C–H	1.10		

Table VI. Extended Hückel Parameters

		H_{ij}	ζ_1	ζ_2	c_1	c_2
Au	6s	−10.92	2.602			
	6p	−5.55	2.584			
	5d	−15.07	6.163	2.794	0.6442	0.5356

		H_{ij}	ζ_1			H_{ij}	ζ_1
S	3s	−20.0	1.817	C	2s	−21.4	1.625
	3p	−13.3	1.817		2p	−11.4	1.625
P	3s	−18.6	1.60	H	1s	−13.6	1.30
	3p	−14.0	1.60				

Acknowledgment. The permanent address of Y.J. is the Institute of Theoretical Chemistry at Jilin University, Changchun, Peoples Republic of China. His stay at Cornell University was made

(21) Teo, B.-K.; Snyder-Robinson, P. A. *Inorg. Chem.* **1981**, *20*, 4235–4239.

possible by NSF Research Grant INT-8117267, supporting the joint research of the groups of A. Tang, J. Lu, J. A. Ibers, and R.H. The permanent address of S.A. is the Departament de Química Inorgànica, Facultat de Química, Universitat de Barcelona, Barcelona, Spain. His stay at Cornell was made possibly by a Fulbright/MEC grant. We are grateful to J. Silvestre for helpful discussions.

Appendix

The average bond distances (Å) and other parameters of $[Au_2S_2PR_2)_2]_n$[10] and $[Au(CH_2)_2PR_2]_2$[12] are listed in Table V.

Our calculations used the extended Hückel method,[21] with weighted H_{ij}'s.[22] The Coulomb integrals and wave functions are specified[5] in Table VI.

Registry No. $[Au_2(S_2PH_2)_2]_2$, 94645-16-6; $[Au_2(S_2PH_2)_2]_x$, 94645-18-8; $Au(S_2PH_2)_2$, 94645-19-9.

(22) Hoffmann, R. *J. Chem. Phys.* **1963**, *39*, 1397-1412.
(23) (a) Ammeter, J. H.; Bürgi, H.-B.; Thibeault, J. C.; Hoffmann, R. *J. Am. Chem. Soc.* **1978**, *100*, 3686-3692. (b) Hoffmann, R.; Hofmann, P. *J. Am. Chem. Soc.* **1976**, *98*, 598-604.

Contribution from the Institut für Physikalische Chemie, Universität Frankfurt, 6000 Frankfurt am Main, Federal Republic of Germany, and Institut de chimie minérale et analytique, Universite de Lausanne, 1005 Lausanne, Switzerland

Associative Nature of Substitution Reactions of Manganese(II) in Aqueous Solution

R. MOHR,[1a] L. A. MIETTA,[1b] Y. DUCOMMUN,[1b] and R. VAN ELDIK*[1a]

Received June 20, 1984

The forward and reverse rate constants for the complex formation of Mn^{2+} with terpy (2,2′:6′,2″-terpyridine) were studied as a function of pressure up to 200 MPa with stopped-flow techniques. From an analysis of the metal ion concentration dependence of the observed rate constant, the calculated volumes of activation are $\Delta V_f^* = -3.4 \pm 0.7$ and $\Delta V_r^* = -7.7 \pm 2.2$ cm^3 mol^{-1} at 288.1 K. The volume of activation for the reverse reaction was also obtained directly by studying the spontaneous aquation of $Mn(terpy)^{2+}$ in the presence of a much better complexing metal ion. The corresponding value is $\Delta V_r^* = -10.1 \pm 0.4$ cm^3 mol^{-1} at 298.1 K. In addition, the overall reaction volume was determined spectrophotometrically from the pressure dependence of the equilibrium constant. These results underline the associative nature of substitution on Mn^{2+} as concluded from the variable-pressure water-exchange data. They further confirm that, in water, the earlier members of the second-row transition-metal series react according to associative activation modes.

Introduction

High-pressure NMR techniques have been applied very successfully in the elucidation of the intimate nature of solvent-exchange processes of solvated transition-metal ions.[2] A remarkable finding is the gradual mechanistic changeover from I_a to I_d for solvent-exchange reactions on divalent first-row transition-metal ions along the series Mn^{2+}, Fe^{2+}, Co^{2+}, and Ni^{2+} for methanol and acetonitrile exchange[3,4] and from V^{2+} to Ni^{2+} for water exchange.[5,6] This contradicts the earlier generally accepted idea that complex formation reactions on all octahedral divalent metal ions proceed via I_d mechanisms. The dissociative character was assigned on the basis of small changes in the substitution rates for a number of ligands of the same charge.[7-10] Obviously, the volume of activation is a more sensitive parameter, leading to a better understanding of the nature of the substitution processes and, therefore, of the chemistry of such metal ions.

Consequently, the question arises as to whether ligand substitution reactions, viz. complex formation and solvolysis processes, also exhibit this mechanistic changeover along the first-row elements. Only a few pressure-dependence studies of such fast substitution reactions have been reported to date. The majority concern complex formation reactions of Co^{2+} and Ni^{2+},[11-19] for which a good correlation with the volume of activation for the solvent-exchange reaction was observed, confirming the I_d character of the substitution processes on these ions. Only two studies[20,21] concern complex formation reactions of V^{2+} and Mn^{2+} (with thiocyanate[20] and bipyridine,[21] respectively), and here again, the reported volumes of activation (-2.1 ± 0.8 and -1.2 ± 0.2 cm^3 mol^{-1}, respectively) parallel the solvent-exchange data, underlining the I_a nature of substitution processes on the early elements of the series.

We have extended our earlier measurements[20,21] and now report volumes of activation as well as reaction-volume data for the formation and aquation reactions of $Mn(terpy)^{2+}$ (terpy = 2,2′:6′,2″-terpyridine) in aqueous solution.

Experimental Section

$Mn(ClO_4)_2 \cdot 6H_2O$, $Co(ClO_4)_2 \cdot 6H_2O$ and terpyridine were used as supplied by Fluka (p.a.). Stock solutions were prepared volumetrically at room temperature with doubly distilled water. The concentrations were not corrected for volume changes with varying temperature or

(1) (a) Universität Frankfurt. (b) Universite de Lausanne.
(2) Merbach, A. E. *Pure Appl. Chem.* **1982**, *54*, 1479.
(3) Meyer, F. K.; Newman, K. E.; Merbach, A. E. *Inorg. Chem.* **1979**, *18*, 2142.
(4) Meyer, F. K.; Newman, K. E.; Merbach, A. E. *J. Am. Chem. Soc.* **1979**, *101*, 5588.
(5) Ducommun, Y.; Newman, K. E.; Merbach, A. E. *Inorg. Chem.* **1980**, *19*, 3696.
(6) Ducommun, Y.; Zbinden, D.; Merbach, A. E. *Helv. Chim. Acta* **1982**, *65*, 1385.
(7) Eigen, M. *Z. Elektrochem.* **1960**, *64*, 115.
(8) Eigen, M. *Pure Appl. Chem.* **1963**, *6*, 97.
(9) Wilkins, R. G.; Eigen, M. *Adv. Chem. Ser.* **1965**, *No. 49*.
(10) Wilkins, R. G. *Acc. Chem. Res.* **1970**, *3*, 408.
(11) Caldin, E. F.; Grant, M. W.; Hasinoff, B. B. *J. Chem. Soc., Faraday Trans. 1* **1972**, *68*, 2247.
(12) Grant, M. W. *J. Chem. Soc., Faraday Trans. 1* **1973**, *69*, 560.
(13) Yu, A. D.; Waissbluth, M. D.; Grieger, R. A. *Rev. Sci. Instrum.* **1973**, *44*, 1390.
(14) Jost, A. *Ber. Bunsenges. Phys. Chem.* **1975**, *79*, 850.
(15) Caldin, E. F.; Greenwood, R. C. *J. Chem. Soc., Faraday Trans. 1* **1981**, *77*, 773.
(16) Inoue, T.; Kojima, K.; Shimozawa, R. *Chem. Lett.* **1981**, 259.
(17) Ishihara, K.; Funahashi, S.; Tanaka, M. *Inorg. Chem.* **1983**, *22*, 2564.
(18) Inoue, T.; Kojima, K.; Shimozawa, R. *Inorg. Chem.* **1983**, *22*, 3972.
(19) Inoue, T.; Sugahara, K.; Kojima, K.; Shimozawa, R. *Inorg. Chem.* **1983**, *22*, 3977.
(20) Nichols, P. J.; Ducommun, Y.; Merbach, A. E. *Inorg. Chem.* **1983**, *22*, 3993.
(21) Doss, R.; van Eldik, R. *Inorg. Chem.* **1982**, *21*, 4108.

0020-1669/85/1324-0757$01.50/0